

Sneaky Spikes: Uncovering Stealthy Backdoor Attacks in Spiking Neural Networks with Neuromorphic Data

Gorka Abad

Radboud University

Ikerlan Research Centre

Oğuzhan Ersoy

Radboud University

Stjepan Picek

Radboud University

Aitor Urbieta

Ikerlan Research Centre

Abstract

Deep neural networks (DNNs) have achieved excellent results in various tasks, including image and speech recognition. However, optimizing the performance of DNNs requires careful tuning of multiple hyperparameters and network parameters via training. High-performance DNNs utilize a large number of parameters, corresponding to high energy consumption during training. To address these limitations, researchers have developed spiking neural networks (SNNs), which are more energy-efficient and can process data in a biologically plausible manner, making them well-suited for tasks involving sensory data processing, i.e., neuromorphic data. Like DNNs, SNNs are vulnerable to various threats, such as adversarial examples and backdoor attacks. Yet, the attacks and countermeasures for SNNs have been almost fully unexplored.

This paper investigates the application of backdoor attacks in SNNs using neuromorphic datasets and different triggers. More precisely, backdoor triggers in neuromorphic data can change their position and color, allowing a larger range of possibilities than common triggers in, e.g., the image domain. We propose different attacks achieving up to 100% attack success rate without noticeable clean accuracy degradation. We also evaluate the stealthiness of the attacks via the structural similarity metric, showing our most powerful attacks being also stealthy. Finally, we adapt the state-of-the-art defenses from the image domain, demonstrating they are not necessarily effective for neuromorphic data resulting in inaccurate performance.

1 Introduction

Deep neural networks (DNNs) have achieved top performance in machine learning tasks in different domains, like computer vision [26], speech recognition [19], and text generation [5]. One key aspect of DNNs that has contributed to their success is their ability to learn from large amounts of data and discover complex patterns. This is achieved through multiple layers of interconnected neurons. The connections between these nodes

are weighted, and the weights are adjusted during training to minimize error and improve the model’s accuracy. DNNs have many hyperparameters that can be tuned to achieve top performance on a given task, but careful optimization of these hyperparameters is crucial. Training a well-performing DNN can be time and energy expensive as it requires tuning an enormous number of parameters with large training data. For example, training the GPT-3 model consumed about 190 000 kWh of electricity [9]. These models’ increasing complexity and computational requirements have led researchers to explore alternative approaches, such as spiking neural networks (SNNs) [11, 13, 16, 43].

SNNs can significantly reduce the energy consumption of neural networks. For instance, Kundu et al. achieved better compute energy efficiency (up to 12.2 \times) compared to DNNs with a similar number of parameters [27]. In addition to their energy efficiency, SNNs have several other benefits. SNNs can be more robust to noise and perturbations, making them more reliable in real-world situations [29]. More precisely, data captured by a Dynamic Vision Sensor (DVS) [41]—which SNNs can process—captures per pixel brightness changes asynchronously, instead of the absolute brightness in a constant rate—as in images. Compared to standard cameras, DVS cameras are low power consumption and capture low latency data, i.e., neuromorphic data, which also has high temporal resolution [8, 32]. Thus, SNNs can process data in a more biologically plausible manner, such as neuromorphic data (see Figure 1), making them well-suited for tasks involving sensory data processing. For example, the computer vision domain has achieved top performance in autonomous driving. A camera (or several) placed in a car captures the surroundings, processed by a DNN. The DNN decisions allow the car to drive autonomously. Recent investigations suggested using event-based neuromorphic vision to achieve the same goal [8, 46]. Event-based data allows solving challenging scenarios where regular cameras cannot perform well [36, 56], such as high-speed scenes, low latency, and low power consumption scenarios. Moreover, SNNs are used in domains like medical diagnosis [15] and computer vision [21, 52]. SNNs

are also implemented on neurosynaptic system platforms like TrueNorth [2]. Finally, while DNNs are often considered to perform better than SNNs in terms of accuracy, recent results show this performance gap is reducing or even disappearing [44].

Neural networks, including DNNs and SNNs, are generally subject to privacy and security attacks, e.g., adversarial examples [42], inference attacks [6], model stealing [24], and backdoor attacks [20]. Backdoor attacks¹ are a threat where malicious samples containing a trigger are included in the dataset at training time. After training, a backdoor model correctly performs the main task at test time while achieving misclassification when the input contains the trigger. Backdoor attacks on DNNs are well studied with several improvements such as stealthy triggers [35, 55] and dynamic triggers unique per data sample [37, 39]. Moreover, there are multiple works considering the backdoor defenses trying to detect and prevent backdoor attacks by inspecting DNN models [33, 47].

The existing backdoor attacks and defenses on DNNs do not directly apply to SNNs because of the different structures of SNNs and their usage of neuromorphic data. Unlike DNNs, SNNs do not have activation functions but spiking neurons, which could reduce or even disable the usage of existing attacks and defenses in DNNs that rely on them, as discussed in Section 4. Additionally, the time-encoded behavior of neuromorphic data allows a broader range of possibilities when generating input perturbations. At the same time, the captured data is encoded in much smaller pixel space (2-bit pixel space) than in regular images, which can handle up to 255-pixel possibilities per channel. The challenges regarding the application of backdoor attacks in SNNs are detailed in Section 3.

To the best of our knowledge, there is only one work exploring backdoor attacks on SNNs [1]. The triggers used in the attack are static and moving square, which is not stealthy and is easily visible by human inspection. Furthermore, their attack setup is limited, only considering three different poisoning rates and a single trigger size. Finally, the authors did not consider any backdoor defense mechanisms.

This paper thoroughly investigates the viability of backdoor attacks in SNNs, the stealthiness of the trigger, and the robustness against the defenses. First, we improve the performance of the static and moving triggers proposed in [1]. Next, we propose two new trigger methods: smart and dynamic triggers. Our novel methods significantly outperform the existing backdoor attacks in SNNs. Our main contributions can be summarized as follows:

- We explore different backdoor injecting methods on SNNs, and all of them achieve (at least) up to 99% accuracy in both main and backdoor tasks. We thoroughly explored static and moving triggers, which led to the development of a smart attack that selects the best location

and color for the trigger.

- Motivated by the knowledge gained from the smart trigger, we present, to the best of our knowledge, the first dynamic backdoor attack on the neuromorphic dataset, which is invisible to human inspection while reaching top performance.
- We analyze the stealthiness of backdoor attacks concerning the structural similarity index (SSIM) metric and show that our dynamic trigger achieves the best stealthiness, up to 99.9 SSIM, while other methods, like static or moving triggers, achieve 98.5% SSIM.
- We adapt state-of-the-art defenses from the image domain into the domain of SNNs and neuromorphic data and compare the effectiveness of each attack method. We observe that existing (adapted) defenses can be ineffective against backdoor attacks in SNNs. Still, we show that retraining the model for a few epochs on clean data helps reduce the backdoor effect while keeping the clean accuracy high.
- We evaluate four trigger methods and three datasets. For each method, we evaluate (i) the success ratio of the attack, (ii) the degradation of the clean model accuracy, (iii) the stealthiness of the trigger, and (iv) the robustness of the attack against the state-of-the-art backdoor defenses.

We share our code to allow the reproducibility of our results.² Moreover, we show the dynamic motion and the stealthiness of our triggers in a demo in the repository.

2 Background

2.1 Backdoor Attacks

Backdoor attacks modify the behavior of a model during training, so at test time, it behaves abnormally [20]. A backdoored model misclassifies the inputs with a trigger while behaving normally on clean inputs. In the image domain, the trigger can be a pixel pattern in a specific part of the image. When the algorithm is trained on a mixture of clean and backdoor data, the model learns only to misclassify the inputs containing the pixel pattern, i.e., the trigger, to a particular target label.

Formally, an algorithm $f_\theta(\cdot)$ is trained on a mixture dataset containing clean and backdoor data, which rate is controlled by $\epsilon = \frac{m}{n}$ where n is the size of the clean dataset, m is the size of the backdoor dataset, and $m \ll n$. The backdoor dataset is composed of backdoor samples $\{(\hat{\mathbf{x}}, \hat{y})\}^m \in \mathcal{D}_{bk}$, where $\hat{\mathbf{x}}$ is the sample containing the trigger and \hat{y} is the target label. For a clean dataset of size n , the training procedure aims to find θ by minimizing the loss function \mathcal{L} :

$$\theta' = \underset{\theta}{\operatorname{argmin}} \sum_{i=0}^n \mathcal{L}(f_\theta(\mathbf{x}_i), y_i), \quad (1)$$

¹We only investigate data poisoning-based backdoor attacks.

²The code will become publicly available after acceptance.

where \mathbf{x} is input and y is label.

During the training with backdoor data, [Equation 1](#) is modified to include the backdoor behavior expressed as:

$$\theta' = \underset{\theta}{\operatorname{argmin}} \sum_{i=0}^n \mathcal{L}(f_{\theta}(\mathbf{x}_i), y_i) + \sum_{j=0}^m \mathcal{L}(f_{\theta}(\hat{\mathbf{x}}_j), \hat{y}_j).$$

2.2 Spiking Neural Networks & Neuromorphic Data

To explain the differences between DNNs and SNNs, let us consider an example with a multilayer perceptron (MLP), which consists of layers containing neurons. The neurons in a layer are connected to all the neurons in the next layer. Each neuron is defined by its weight and bias. Therefore, an input is transformed by each neuron at different layers. Often the bias is set to 1, so the incoming value always propagates to the next layer, i.e., all neurons send a value to the next layer. The explained architecture is linear, making it difficult to train. However, including activation functions between neurons converts the algorithm into a piece-wise linear function. Commonly, the Rectified Linear Unit (ReLU) activation function is used:

$$h(x) = \begin{cases} x, & \text{if } x \geq 0 \\ 0, & \text{otherwise} \end{cases}$$

In SNNs, instead of neurons, *spiking neurons* are used. SNNs have the same structure as DNNs; however, spiking neurons require excitation up to some threshold to fire, allowing the inputs of a spiking neuron to go through. Spiking neurons are excited by the incoming inputs, which excitation adds up over time to some threshold that lets the transformed input go to the next spiking neuron(s). Once the threshold (Θ) is reached, the spiking neuron is fired, and the excitation value gets reset; otherwise, the neuron's activation decays over time. Therefore, SNNs are non-linear by design due to the fire-and-reset process:

$$h(x) = \begin{cases} 1, & \text{if } x \geq \Theta \\ 0, & \text{otherwise.} \end{cases}$$

SNNs commonly work with neuromorphic data, a time-encoded representation of the illumination changes of an object/subject captured by a DVS camera. A DVS camera captures a flow of spiking events that dynamically represents the changing visual scene. An advantage of DVS cameras is that they provide an almost instantaneous representation of the visual scene in a very compressed form, which facilitates posterior data processing. Precisely, neuromorphic data is encoded in T frames and p polarities, i.e., *ON polarity* and *OFF polarity*, which represent the changes in the visual scene. As an example, we divide the data points into $T = 16$ frames, where each polarity generates a color, as seen in [Figure 1](#).

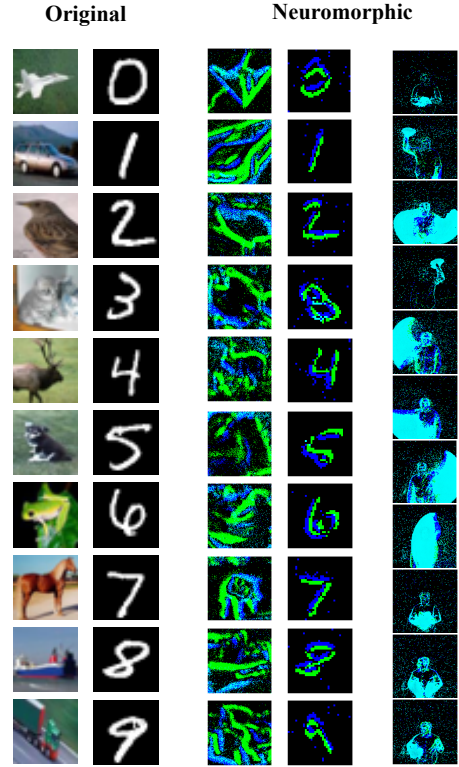


Figure 1: Normal and neuromorphic data samples. The first two columns show examples from the CIFAR-10 and MNIST datasets, and the following two are their neuromorphic versions. The last column is from the DVS128 Gesture dataset, which is originally neuromorphic (see Section 4).

3 Backdoor Attacks to SNNs

3.1 Threat Model

We consider a *white-box* attack where the attacker has access to the entire training procedure and the training dataset. We assume a *dirty-label* backdoor where the attacker can alter the training samples and their labels. Even though this threat model is weaker than its counterpart, i.e., *clean-label* attack [45], it is the most common in the literature [20, 37, 39]. Finally, we target only scratch-trained models.

As a use case, we assume that a client wants to train an SNN on an owned dataset but does not have the resources, e.g., GPU cards, to train it. Therefore, the client outsources the training to a third party that provides on-cloud training services, such as Google Cloud or Amazon Web Services, by sharing the model architecture and the training dataset. We assume that the attacker is the third-party provider, thus having access to the training procedure, the model, and the dataset. The attacker then injects the backdoor during training and shares the model with the client. The client can check the model's performance using a holdout dataset.

3.2 Challenges in SNNs

SNNs have a different network structure than DNNs and utilize neuromorphic datasets. However, the information propagation approach is the key difference between “classical” DNNs and SNNs. SNNs do not work with continuously changing time values (like DNNs) but operate with discrete events that occur at certain points in time. Thus, the training is different, making the attacks happening in the training phase (potentially) challenging to deploy. For instance, the triggers used in the image domain are encoded in 255 possibilities per channel, which gives many combinations of color to be. In neuromorphic data, however, the trigger space is reduced to 4 possibilities encoded by the two different polarities. Furthermore, in the image domain, the trigger is commonly static, i.e., no time-encoded data is used. In neuromorphic data, we encode the trigger using the time window, allowing us to create triggers that change the location through time. Next, we list the main challenges:

C.1: Designing and optimizing the trigger. Because of having several frames per data point, the triggers can vary their position, shape, polarities, etc., through time. The large set of possibilities leads to the following questions: How can we efficiently select the trigger that would maximize the attack performance while having minimal influence on the clean accuracy drop? How can we decide on the most important parameters for a neuromorphic backdoor trigger in SNNs?

C.2: Generating stealthy triggers. Since each pixel of a neuromorphic trigger can only take four different values, smoothing the trigger over the clean data is challenging compared to images with, e.g., 3×256 values. The limitation yields the following questions: How can we design a backdoor trigger that exploits the time-encoded data to generate an invisible trigger unique per input sample and frame? How will the chosen parameters affect the trigger stealthiness?

C.3: Backdoor defenses. Since SNNs do not have activation functions, which are commonly utilized in backdoor defenses, the state-of-the-art defenses may not apply to SNNs. Moreover, the defenses are commonly designed for images, whereas neuromorphic data consists of several frames per data point. These differences lead to the following questions: How successful are the existing defenses against SNNs? How can we adapt the defenses for datasets with multiple frames?

C.4: Assessing stealthiness. It is non-trivial to assess the stealthiness of a backdoor trigger via a subjective human perspective, which leads to the following question: How can we objectively assess the stealthiness of a trigger for neuromorphic data?

Knowing the limitations in color and the flexibility in changes through time, we propose different techniques for injecting a backdoor in SNNs. With this information, we improve two attacks: static and moving backdoors, and we propose two novel attacks: smart and dynamic backdoors.

3.3 Static Backdoor

Backdoor attacks in SNNs or neuromorphic data were not explored before the work of Abad et al. [1]. Inspired by backdoor attacks in the image domain [20], the authors replicated the square trigger used in neuromorphic data. By completely discarding the time-encoded advantages neuromorphic data have, the authors included the same trigger (same position and polarity) in all the frames, thus making a static trigger. In this section, we also investigate this trigger type as a baseline for subsequent ones, thoroughly investigating the trigger position, polarity, and size in a wide range of cases.

We follow the same intuition of a pixel-squared trigger of a given color, which is now set by the polarity for neuromorphic data. The data samples contain two polarity values, either *ON polarity* or *OFF polarity* corresponding to the black and light blue. However, when pixels from different polarities are overlapped, it generates another two color polarities, i.e., dark blue and green. The polarity p in neuromorphic datasets is a two-bit discrete value, creating up to four different combinations; we rename the polarities for simplicity to p_0, p_1, p_2 , and p_3 . Thus, the trigger gets a different color for different polarity combinations, i.e., black, dark blue, green, or light blue. The trigger can be placed in a specific location of the input: top-right, middle, bottom-left, random, or any other desired location l , see Figure 2 as an example. For our attacks, we also consider the trigger size, s , as the percentage of the input size, for constructing the trigger. Still, the input samples are divided into T frames, so the trigger k is replicated for each frame and sample, i.e., the trigger does not change the location. Consequently, it is static.

We consider all discussed parameters in the backdoor creation function $\mathcal{A}(\mathbf{x}, p, s, l)$ for creating a set of backdoor samples $\mathcal{D}_{bk} : \hat{\mathbf{x}} \in \mathcal{D}_{bk}$ containing the trigger k . By controlling ϵ value $\epsilon = \frac{m}{n}; m \ll n$ with n the size of \mathcal{D}_{clean} and m the size of \mathcal{D}_{bk} , the attacker controls the amount of backdoored data during training.

3.4 Moving Backdoor

As previously seen, static backdoors replicate the trigger from backdoor triggers in the image domain. However, a unique characteristic of neuromorphic data allows the attacker to develop a better version of the trigger. To this end, moving triggers inject a trigger per frame in different locations, exploiting the time-encoded nature of neuromorphic data. The nature of neuromorphic data is driven by polarity, i.e., movement, which contradicts the static behavior of the naïve static attack. Driven by this discrepancy and the aim of creating a more stealthy attack that cannot be detected easily by human inspection (more about attack stealthiness is in Section 5), we consider a more robust approach, named moving backdoor, improving previous work [1].

The moving backdoor primary leverages the “motion” na-

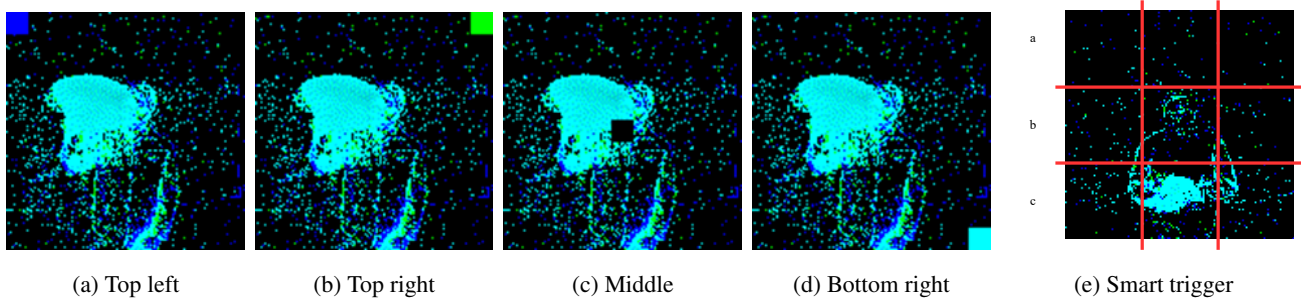


Figure 2: Input samples containing a static trigger (2a, 2b, 2c, and 2d) and a smart backdoor mask for $n = 2$ (2e).

ture of neuromorphic datasets for creating moving triggers that move along the input. Precisely, for a given polarity p , a location l , and size s , the trigger k smoothly changes from frame to frame, creating a moving effect. Formally, the backdoor creation function takes the parameters mentioned above $\mathcal{A}(\mathbf{x}, p, s, l, T)$ for creating a backdoor set of inputs \mathcal{D}_{bk} , where T is the total amount of frames that the input is divided.

The backdoor creation function also considers the number of frames T , such that for each frame, $\mathcal{A}(\cdot)$ calculates a location at $t + 1 \in T$ close to the previous frame t . This allows the trigger to simulate a smooth movement in the input space. Unlike the static trigger, the moving trigger can be placed on top of the input “activity area” for better stealthiness. Additional information about stealthiness can be found in Section 5. In our investigation and contrary to [1], we consider a wide experimental setup. Additionally, we analytically measure and compare the stealthiness of static and moving backdoor. Finally, we also compare these attacks against the implemented defenses.

3.5 Smart Backdoor

So far, the proposed techniques, i.e., static and moving backdoors, inject the backdoor in the model correctly, even improving the attack stealthiness in the latter case. With the *smart backdoor* approach, we aim to optimize the backdoor performance, simplicity, stealthiness, and understanding by removing the two hyperparameters, namely the polarity p and trigger location l . For a better understanding of the effects of the trigger location, we split the image by drawing n vertical and horizontal lines (see Figure 2e). These will divide the image into $(n+1)^2$ chunks, which we call *masks*. Note that a larger n value would create more masks, allowing the attacker to have more control over the “optimal” spot of trigger placement. We discuss its effectiveness in Section 4. The smart backdoor attacks leverage the inputs’ polarity changes to find the most *active mask*. We define the *mask activation* as the sum of all the polarity changes happening in a mask for all the frames, excluding the polarity p_0 , which represents no movement, i.e., the black color or the background. This way,

the smart backdoor finds the most active mask in the input sample. Formally, given a set of masks, \mathcal{S}_{mask} the most active mask is found by

$$v' = \operatorname{argmax}_{v \in \mathcal{S}_{mask}} \sum_{i=0}^{(n+1)^2} p_1^i + p_2^i + p_3^i,$$

where p_1, p_2 , and p_3 are different polarities. For example, in Figure 2e, $n = 2$ lines horizontally and vertically split the image into nine masks. The smart attack will decide which mask is the most active, the “2,c” mask in this case.³

Once the location is chosen, the smart backdoor attack also selects the best polarity for the trigger, backdoor performance-wise, i.e., the least used polarity in the mask. Formally, the polarity p' is selected, given

$$p' = \operatorname{argmin}_{p \in \llbracket 0, 3 \rrbracket} \sum_{i=0}^3 v(p_i).$$

Therefore, p' is used for the polarity of the trigger k and is injected in v' , randomly and smoothly moving around the mask for all the frames.

Note that the trigger polarity p' and the mask v' are calculated for the poisoned dataset m , i.e., all the poisoned samples have the same trigger location and polarity. Formally, the smart backdoor creation function is defined as $\mathcal{A}(\mathbf{x}, p', v', T)$, generating a set of moving triggers that are combined with the clean samples to create a set of poisoned samples \mathcal{D}_{bk} .

Additionally, we investigate the effect of injecting the trigger in the least active masks, such as

$$v' = \operatorname{argmin}_{v \in \mathcal{S}_{mask}} \sum_{i=0}^{(n+1)^2} p_1^i + p_2^i + p_3^i,$$

and we consider the usage of the most used polarity in the mask defined as

$$p' = \operatorname{argmax}_{p \in \llbracket 0, 3 \rrbracket} \sum_{i=0}^3 v(p_i).$$

³We also investigate the effect of injection of the trigger in the least active area in Section 4.

3.6 Dynamic Backdoor

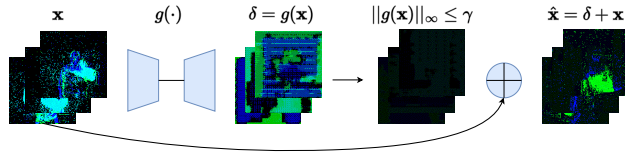


Figure 3: Overview of the dynamic moving attack.

Having explored how to inject a backdoor in SNNs using static triggers, exploiting the time-encoded nature of neuromorphic data with moving backdoors, and optimizing the trigger polarity and location with the smart trigger, we propose a stealthy, invisible, and dynamic trigger. More precisely, motivated by dynamic backdoors in the image domain [10, 37], we investigate *dynamic moving backdoors* where the triggers are invisible, unique for each image and frame, i.e., the trigger changes from frame to frame. To achieve this, we use a spiking autoencoder to generate the optimal noise, as big as the image, which maximizes the backdoor performance, maintains a clean accuracy, and is invisible. More precisely, one of the weakest points of the previous backdoor triggers is that they are detectable under human inspection. Therefore, we aim to create an invisible trigger. For example, autoencoders are used for denoising tasks, where we would usually require clean (denoised) and noisy versions of the image to train the autoencoder, i.e., the autoencoder is trained on image pairs. However, we do not have the clean image and trigger pair to train the autoencoder for our attack. If we had the trigger, there would be no need for the autoencoder. Therefore, to fulfill these requirements, we must train the model and the autoencoder simultaneously to make the autoencoder generate a trigger unique for each sample. Contrary to previous work [10], we do not need a fine-tuning phase to achieve a successful backdoor model.

Intuitively, the dynamic backdoor is designed as follows (see Figure 3). At first, we generate the perturbation by passing a clean image to the spiking autoencoder $g(\cdot)$: $\delta = g(\mathbf{x})$. The perturbation is then added to the clean image to construct a backdoor image $\hat{\mathbf{x}} = \mathbf{x} + \delta$. However, this naïve approach would saturate \mathbf{x} with δ , which makes the trigger visible. Thus, we project the perturbation to a l_p -ball of a given budget γ : $\|g(\mathbf{x})\|_\infty \leq \gamma$. Then, $g(\cdot)$ is updated aiming to maximize the backdoor accuracy of $f(\cdot)$, thus during training $g(\cdot)$ optimizes the parameters ζ that minimize the given loss function:

$$\zeta' = \operatorname{argmin}_{\zeta} \sum_{i=0}^n \mathcal{L}(f_\theta(g_\zeta(\mathbf{x}_i) + \mathbf{x}_i), \hat{y}_i), \\ \text{s.t. } \|g_\zeta(\mathbf{x})\|_\infty \leq \gamma \quad \forall \mathbf{x}, \quad (2)$$

where \hat{y} is the target label, n is the length of the dataset, and \mathcal{L} is a loss function, mean squared error in our case.

For training $f(\cdot)$, the parameters θ are updated by minimizing

$$\theta' = \operatorname{argmin}_{\theta} \sum_{i=0}^n \alpha \mathcal{L}(f_\theta(\mathbf{x}_i), y_i) + \\ (1 - \alpha) \mathcal{L}(f_\theta(g_\zeta(\mathbf{x}_i) + \mathbf{x}_i), \hat{y}_i), \\ \text{s.t. } \|g_\zeta(\mathbf{x})\|_\infty \leq \gamma \quad \forall \mathbf{x}, \quad (3)$$

where α controls the trade-off between the clean and the backdoor performance, a large α as 1 is equivalent to training $f(\cdot)$ only with clean data. γ controls the visibility of the trigger. We discuss the influence of α and γ in Section 4, where α controls the trade-off between the clean and the backdoor performance, a large α as 1 is equivalent to training $f(\cdot)$ only with clean data. Indeed, γ controls the visibility of the trigger.

4 Evaluation

Datasets We use three datasets: N-MNIST [38], CIFAR10-DVS [30], and DVS128 Gesture [3]. We use N-MNIST and CIFAR10-DVS because the non-neuromorphic version of them are the most common benchmarking datasets in computer vision for security/privacy in ML. The DVS128 Gesture dataset is a “fully neuromorphic” dataset created for SNN tasks. N-MNIST is a spiking version of MNIST [28], which contains 34×34 60 000 training, and 10 000 test samples. An ATIS sensor captured the dataset across the 10 MNIST digits shown on an LCD monitor. The CIFAR10-DVS dataset is also a spiking version of the CIFAR10 [25] dataset, which contains 60 000 training, and 10 000 test 128×128 samples, corresponding to 10 classes. Lastly, the DVS128 Gesture dataset collects real-time motion captures from 29 subjects making 11 different hand gestures under three illumination conditions, creating a total of 1 176 128×128 training samples, and 288 test samples. All the datasets samples’ shape is $T \times P \times H \times W$, where T is the time steps (we set it to $T = 16$), P is the polarity, H is the height, and W is the width.

Network Architectures We consider three network architectures for the victim classifiers used in related works [13]. The N-MNIST dataset’s network comprises a single convolutional layer and a fully connected layer. For the CIFAR10-DVS dataset, the network contains two convolutional layers followed by batch normalization and max pooling layers. Then two fully connected layers with dropout are added, and lastly, a voting layer—for improving the classification robustness [13]—of size ten is incorporated. Finally, for the DVS128 Gesture dataset, five convolutional layers with batch normalization and max pooling, two fully connected layers with dropout, and a voting layer compose the network.

The spiking autoencoder for the dynamic attack has four convolutional layers with batch normalization, four deconvolutional layers with batch normalization, and tanh as the activation function for the DVS128 Gesture and CIFAR10-DVS datasets. For N-MNIST, we use two convolutional and

two deconvolutional layers with batch normalization and \tanh as the activation function, which is the common structure for an autoencoder [18].

Default Training Settings For training, we set a default learning rate (LR) of 0.001, mean squared error (MSE) as the loss function, Adam as the optimizer, and we split the neuromorphic datasets in $T = 16$ frames using the Spiking-Jelly framework [12]. For the N-MNIST dataset, we achieve a (clean) accuracy of 99% on a holdout test set in 10 epochs. For the CIFAR10-DVS case, we achieve 68% accuracy on 28 epochs and a 93% accuracy on 64 epochs for the DVS128 Gesture dataset. The results are aligned with the state-of-the-art results [40]. A summary can be found in Table 1.

Table 1: Baseline training results for different datasets.

Dataset	# Epochs	Accuracy (%)
N-MNIST	10	99.4 \pm 0.06
CIFAR10-DVS	28	68.3 \pm 0.28
DVS128 Gesture	64	92.5 \pm 0.91

4.1 Experimental Results

In this section, we provide the results for four different attacks, emphasizing their strong and weak points. We use the same training settings as in Section 4.

We evaluate the attacks with the commonly used metrics:

- **Attack success rate (ASR)** measures the backdoor performance of the model based on a holdout fully backdoored dataset.
- Model utility or **clean accuracy** is the performance of the model test on a holdout clean dataset.
- **Clean accuracy degradation** is the accuracy drop (in percentage) from the clean and backdoor models. It is calculated as $\frac{V_2 - V_1}{V_1} \times 100$, where V_1 is the clean baseline accuracy, and V_2 is the clean accuracy after the attack.

4.1.1 Static Backdoor

To first evaluate the viability of backdoors attacks in SNNs, we explore the basic BadNets [20] approach by placing a static trigger in different locations of the input space, various ϵ values with different trigger sizes, and polarities. We test the static attack with ϵ values of 0.001, 0.005, 0.01, 0.05, and 0.1. We set the trigger sizes to 1% and 10% of the input image size. Lastly, we experiment with three trigger locations: bottom-right, middle, and top-left, and four different polarities.

Our results show that static backdoors require a trigger size as big as 10% of the input size to inject the backdoor behavior in complex datasets like CIFAR10-DVS or DVS128 Gesture. When the trigger is 1% of the input size, the backdoor is only injected in N-MNIST when the polarity is different from 0. However, when the trigger is in the middle, we observe that $p = 0$ gets up to 100% ASR. This is caused because

the data is centered; thus, the black trigger is on top of the image, contrasting and allowing the model to distinguish the trigger. In subsequent sections, we further investigate the importance of injecting the trigger in the most important or least important location. Increasing the trigger size makes the backdoor achieve an excellent ASR (up to 100%) when the trigger is placed in the corners. See Figure 8a, Figure 8b, and Figure 8c, for the results of bottom-right, middle, and bottom-right placed triggers.

Since the DVS128 Gesture dataset is small, the ϵ value drastically affects ASR. When $\epsilon = 0.01$, only a single sample will contain the trigger, which is insufficient to inject the backdoor when the trigger size is small. We further experiment with a larger trigger size, i.e., 0.3, achieving 99% ASR with $\epsilon = 0.01$, in the top left, and using the background polarity. CIFAR10-DVS achieves 100% ASR in all the setting when the trigger size and the poisoning rate are 0.1. CIFAR10-DVS is the only dataset that achieves 100% ASR in the bottom right, with the polarity 0. This is caused by the dataset itself, which is noisy; thus, the black trigger can contrast with the background.

Regarding the clean accuracy degradation, we notice a slight degradation in most cases concerning the clean accuracy baseline. See Figure 10, Figure 11, and Figure 12, for the results of the clean accuracy degradation of bottom-right, middle, and bottom-right placed triggers. N-MNIST does not show any significant degradation, while DVS128 Gesture and CIFAR10-DVS are more prone to degrade the main task up to 10%. Overall, static backdoors in SNNs show excellent performance (due to detailed experimentation, even better than [1]). However, they can be easily detected by human investigation (or by automated tools). Specifically, placing a static trigger in a moving input is unnatural, and it could be detected by checking if a part of the image is not moving or by inspecting changes in polarity between pixels. We address this limitation in consequent sections.

4.1.2 Moving Backdoor

We investigate the effect of moving triggers to overcome the stationary behavior of static backdoor attacks. Moving backdoors change the trigger position per frame horizontally, moving in a constant loop. We experiment with the same setting as static backdoors. However, the trigger location varies in time by horizontally moving using top-left, middle, and bottom-right as initial locations. The trigger changes location in two pixels every frame. Thus, the triggers change 16 times in our experiments.

We observe that moving the backdoor overcomes the limitation of static triggers when placed on top of the image action. Since the trigger is moving, it is not always on top of the active area, thus allowing the model to capture both clean and backdoor features. Interestingly, as seen in Figure 9a and contrary to the static backdoor (see Figure 8a), triggers

in the bottom-right corner with background polarity do not work with complex datasets because they merge better with the image, making it impossible for the model to recognize them. However, in N-MNIST, we can achieve 100% ASR with $p \neq 0$ and large ϵ . Moreover, triggers with background polarity in the bottom-right position do not inject the backdoor successfully for the DVS128 Gesture dataset, contrary to static backdoors. That effect is intuitively explained as moving backdoors are more difficult to inject than static ones. The model has to find a more complex relation between the trigger, samples, and label, thus, requiring large datasets.

We observe the opposite behavior with triggers in the top-left corner (see [Figure 9c](#)). We investigate the data samples and conclude that images are usually centered; thus, the main action of the image is also in the middle of the image. In the case of DVS128 Gesture or CIFAR10-DVS, the action is also contained in some corners of the image. From here, we can intuitively explain that injecting the trigger in an active or inactive area of the image could enable or disable the backdoor effect. We investigate the backdoor effect when placing the trigger in the most and least active areas in [Section 4.1.3](#). Lastly, by placing the triggers in the middle (see [Figure 9b](#)), we observe that the DVS128 Gesture dataset achieves 100% ASR when polarity is 1 or 2. These results also suggest that the trigger’s polarity strongly affects the backdoor’s performance. Furthermore, depending on where the trigger is placed, a given polarity could have a different effect, as observed with polarity 2 in [Figure 9b](#) and [Figure 9a](#) for the DVS128 Gesture dataset. [Section 4.1.3](#) investigates this effect in more detail.

Regarding the clean accuracy degradation, we notice a slight degradation in most cases concerning the clean accuracy baseline and an improvement in the clean accuracy in some other settings. See [Figure 13](#), [Figure 14](#), and [Figure 15](#), for the results of the clean accuracy degradation of bottom-right, middle, and bottom-right placed triggers. N-MNIST does not show any degradation, while DVS128 Gesture and CIFAR10-DVS are more prone to degrade the main task up to 7%, contrary to static triggers, which may degrade the clean accuracy up to 10%. We believe this happens as those datasets are more complex, and adding backdoors makes the main task more challenging.

4.1.3 Smart Backdoor

To explore the effects of the trigger location and the trigger polarity, we designed a novel attack that chooses the best combination of both. The smart attack removes the trigger location and the polarity selection by choosing either the most active or least active area of the image. Then, it chooses the least or most common polarity in that mask, where the least common polarity would contrast while the most common one would be more stealthy—enabling a more optimized attack. We experiment with different settings, such as poisoning rates, trigger sizes, and most and least active masks. We also inves-

tigate the trigger polarity’s effect using the most/least active polarity in the selected mask. We split the image using $n = 2$, see [Figure 2e](#).

We observe that the backdoor is not successful with the DVS128 Gesture dataset. The few samples in the dataset make the choice of the most/least active mask of the image not precise. Note that the activity sum is done over all the images in the training set. The more samples, the more precise the selected mask is. Experimentation using the most active area shows excellent performance when the least common trigger polarity is used; see [Figure 4a](#). Intuitively, the least common trigger polarity is preferred to increase ASR because of the trigger contrast compared to the background image.

Using 1% of the image size for the trigger only shows promising results with N-MNIST with $\epsilon = 0.1$. A larger trigger size improves the backdoor success using the least poisoned samples. Interestingly, injecting the trigger in the least active area with the least active trigger polarity, see [Figure 4b](#), shows excellent backdoor performance even with a small trigger size. Finally, experimenting with the most active trigger polarities shows that the trigger merges with the actual image, not allowing the model to capture both the clean image and the trigger, see [Figure 4c](#) and [Figure 4d](#).

Finding. The triggers are best injected in the most active area with the least common polarity.

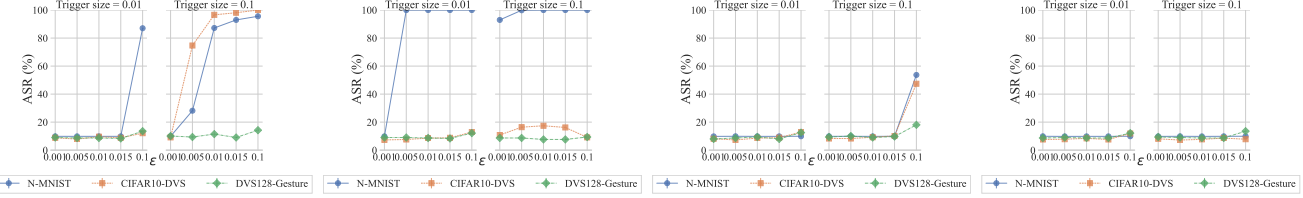
We also experiment with the clean accuracy degradation with the smart trigger. As shown in [Figure 16](#), [Figure 17](#), [Figure 18](#), and [Figure 19](#), we observe a maximum of 4% degradation when the trigger size is 0.01 and the poisoning rate 0.1 for the most active area. Results also show that when the trigger size is more prominent, the clean accuracy drop is negligible in all the cases, even improving it slightly. Injecting the trigger in the least active area shows similar performance; however, the maximum degradation is less. This could be caused by the trigger not overlapping the active area, allowing the model to capture both tasks. This addresses [Challenge C.1](#).

4.1.4 Dynamic Backdoor

Lastly, we experiment with the dynamic moving backdoor. We consider different α (clean backdoor trade-off) and γ (trigger intensity) values, ranging from 0.5 to 0.8 and 0.01 to 0.1, respectively. The clean and backdoor accuracies are measured at the best epochs, selected based on [Algorithm 1](#), prioritizing high ASR instead of maintaining high clean accuracy. Thus, we expect a more significant standard error in the results as we measure the clean accuracies in different epochs.

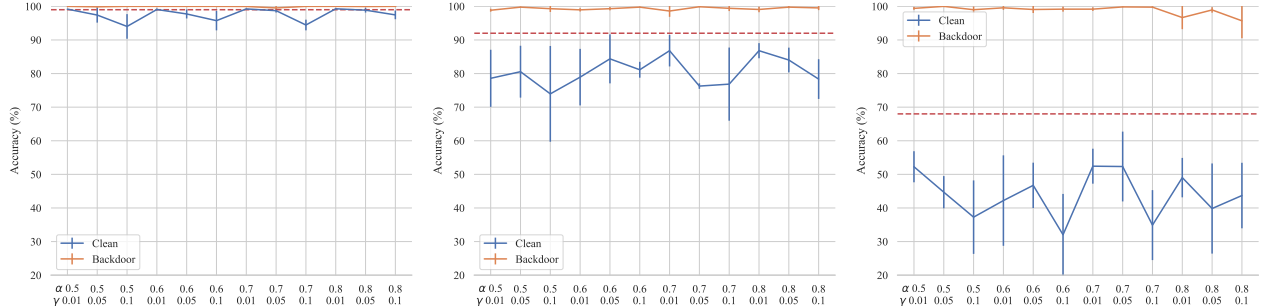
As seen in [Figure 5a](#), for N-MNIST, our dynamic attack achieves 100% ASR in all the settings tested while maintaining the clean accuracy the same, i.e., there is no clean accuracy degradation when γ is small. We experiment with a more noticeable clean accuracy degradation as γ gets larger.

With a more complex dataset, using DVS128 Gesture (see [Figure 5b](#)), we achieve at least 99% ASR. However,



(a) Most active area and least active trigger polarity. (b) Least active area and least active trigger polarity. (c) Most active area and most active trigger polarity. (d) Least active area and most active trigger polarity.

Figure 4: Smart triggers.



(a) Dynamic triggers on N-MNIST. (b) Dynamic triggers on DVS128 Gesture. (c) Dynamic triggers on CIFAR10-DVS.

Figure 5: ASR and clean accuracy degradation of dynamic triggers.

Algorithm 1 Stopping criteria

```

 $acc' \leftarrow 0$             $\triangleright$  Initialize the best clean accuracy and ASR to 0.
 $asr' \leftarrow 0$ 
 $epoch' \leftarrow 0$ 
while  $i \leq epochs$  do
     $acc, asr \leftarrow train()$             $\triangleright$  Train  $f(\cdot)$  and  $g(\cdot)$ 
    if  $acc \geq acc'$  or ( $acc \geq acc'$  and  $asr' \leq asr$ ) then
         $acc' \leftarrow acc$ 
         $asr' \leftarrow asr$ 
         $epoch' \leftarrow epoch$ 
    end if
end while

```

we see a slight degradation in the clean accuracy either when the α value is close to 0.5, i.e., the clean and backdoor task have the same importance, or when the γ value is large, i.e., the perturbation is more intense. Lastly, we observe lower performance in CIFAR10-DVS (see Figure 5c). Indeed, we achieve close to 100% ASR in most settings and a minimum of 90% ASR with $\alpha = 0.8$ and $\gamma = 0.05$. Regarding the clean accuracy, we see a noticeable degradation when (i) γ is large and (ii) the dataset is complex. To our knowledge, the state-of-the-art (clean) accuracy on CIFAR10-DVS is 69.2% [40]. The accuracy is not high; indeed, the model is not thoroughly learning the representation of the dataset, and thus including more complexity with the attack lowers its performance even more. We also observe a better performance with $\alpha = 0.5$ and

$\gamma = 0.01$, where the trigger is subtle—and does not degrade the model much.

To achieve a successful attack, we observe that no matter the setting, ASR is mainly close to 100%. However, to achieve a good trade-off between clean accuracy degradation and trigger invisibility, the attacker should carefully choose α and γ values, specifically γ control the invisibility of the backdoor image, being completely indistinguishable from the clean image when $\gamma = 0.01$. This addresses Challenge C.2.

Finding. An invisible trigger that cannot be detected by humans can be generated using $\gamma = 0.01$.

4.2 Evaluating State-of-the-Art Defenses

In this section, and due to the lack of specially crafted countermeasures for SNNs, we discuss state-of-the-art backdoor defenses in DNNs, and how they are adapted to SNNs and neuromorphic datasets. As discussed in the following sections, defenses for DNNs have core problems since they are based on DL assumptions or consider regular static data. We select two representative defenses based on model inspection: Artificial Brain Stimulation (ABS) [33] and fine-pruning [31].

4.2.1 ABS

The ABS method, as introduced in Liu et al. [33], is a method for identifying backdoors in neural networks using a model-based approach. It works by stimulating neurons in a specific

layer and examining the resulting outputs for deviations from expected behavior. ABS is based on the idea that a class can be represented as a subspace within a feature space and that a backdoored class will create a distinct subspace throughout the feature space. Therefore, ABS hypothesizes that a poisoned neuron activated with a target input will tend to produce a larger output than a non-poisoned neuron.

We adapt ABS to handle neuromorphic data and SNNs. Specifically, we modify the code to process all frames of an image together rather than treating each frame individually since neuromorphic data contains time-encoded information. However, ABS also does not support dynamic, moving, or smart triggers, which are types of backdoors that can change position or be unique to each image. Since the trigger position changes could be interpreted as multi-trigger backdoors—attacks that contain more than one trigger within a single input—which ABS cannot handle. Additionally, dynamic backdoors present a twofold problem for ABS. First, dynamic triggers can also be interpreted as multi-trigger. Second, ABS requires the trigger to be the same every time, i.e., the trigger is not unique per sample. However, the dynamic attack creates input-specific triggers, which can surpass ABS from its core design.

We observe several false positives when testing ABS against static backdoors. When applied to a clean model, ABS marked it as compromised, and when applied to a poisoned model, ABS identified it as compromised but with the wrong target class. This behavior was consistent across all datasets. One possible explanation for this issue is the core assumption of ABS. ABS relies on “turn-points” created by the activation functions in the model, such as ReLU. However, the lack of ReLU activation functions in SNNs makes ABS malfunction, providing inaccurate results.

4.2.2 Fine-pruning

Fine-pruning [31] is a defense mechanism against backdoor attacks composed of two parts: pruning and fine-tuning. Existing works show that by removing (pruning) some neurons of a DNN, the efficiency of DNNs improves while the prediction capacity remains equal [22, 53]. The authors suggested that some neurons may contain the primary task information, others the backdoor behavior, and the rest a combination of main and backdoor behavior. Thus, the backdoor could be completely removed by removing the neurons containing the malicious information. The authors proposed ranking the neurons in the last convolutional layer based on their activation values by querying some data. A pruning rate τ controls the number of neurons to prune. The second part of the defense is fine-tuning. Fine-tuning consists of retraining the (pruned) model for some (small) number of epochs on clean data. By doing this, the model could (i) recover its dropped accuracy during pruning and (ii) altogether remove the backdoor effect. The authors showed that by combining these two, the ASR of

a poisoned model could drop from 99% to 0%.

We implement this defense for SNNs and adapt it to work with neuromorphic data. We investigate the effect of pruning, fine-pruning (pruning + fine-tuning), and solely fine-tuning (when the pruning rate is 0). We also investigate various pruning rates, i.e., $\tau = \{0.0, 0.1, 0.3, 0.5, 0.8\}$ and analyze their impact, see Figure 6. Analyzing the results, we observe that pruning alone does not work. We notice that the clean accuracy drops drastically while ASR remains high, for example, as seen in Figure 6a. Depending on the trigger type, the drop in the clean accuracy is not that severe, but ASR remains high, as seen in Figure 6g. When combining pruning with a fine-tuning phase, i.e., fine-pruning, we observe that ASR can be drastically reduced while the clean accuracy remains high. However, the effect can be similar when focusing solely on the effect of fine-tuning, i.e., no pruned neurons ($\tau = 0$). Thus, pruning will not necessarily affect the model’s backdoor performance. However, we find that solely retraining the model with clean data reduces the backdoor effect. We conclude that fine-tuning could effectively reduce the backdoor performance while keeping clean accuracy high. Still, we note that the effect is more pronounced for backdoors that aim to be more stealthy, making it an interesting trade-off. Since neuromorphic data consists of several frames (16), we are able to inject a moving backdoor, which is not possible in a single image. According to our experimental results shown in Figure 6d, we postulate that fine-pruning may fail to reduce the effect of the moving trigger.

Finding. Fine-pruning can be effective against backdoor attacks in SNNs using neuromorphic data. Still, this depends on the dataset characteristics and the trigger type.

The performance of ABS in detecting backdoors in neuromorphic data and SNNs is limited by its inability to handle dynamic, moving, and smart triggers and its reliance on activation functions not present in SNNs. Further research and development are necessary to address these limitations and improve the robustness of ABS in these contexts. Specific countermeasures considering the nature of neuromorphic data and SNNs are necessary to detect and defend against these backdoors effectively. This addresses Challenge C.3.

5 Stealthiness Evaluation

Quantifying image quality is often used for applications where the end user is a human. Subjective evaluation is often unsuitable for specific applications due to time constraints or expensive costs. This section discusses different state-of-the-art metrics used for quantifying image quality, which we would use for measuring the stealthiness, i.e., variation for the clean input of our backdoor attacks.

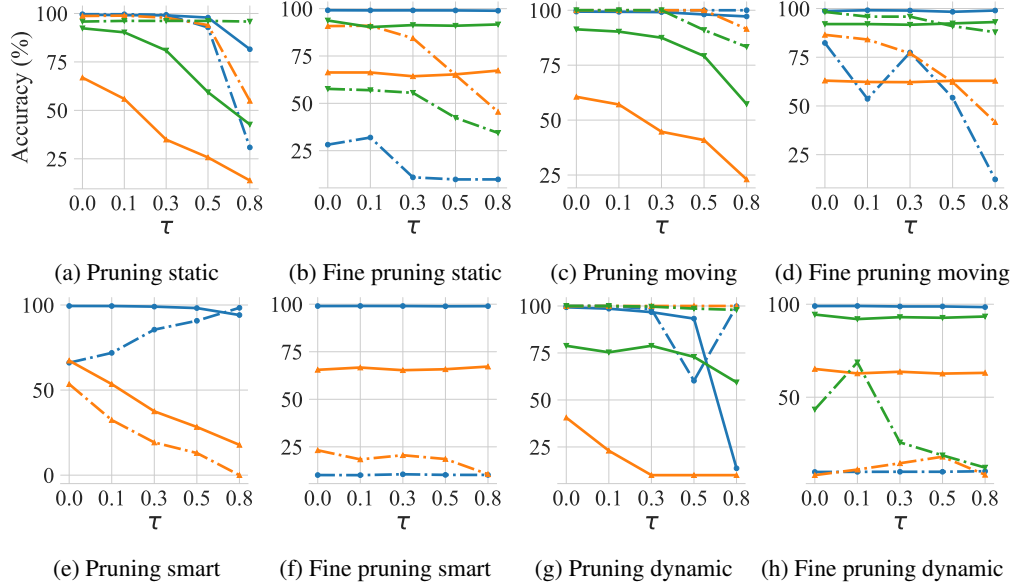


Figure 6: Effect of pruning and fine pruning on the ASR (dashed lines) and clean accuracy (full line) for different types of triggers. Blue corresponds to N-MNIST, orange to CIFAR10-DVS, and green to the DVS128 Gesture dataset.

5.1 Proposed Metrics

Mean squared error [48] (MSE) compares two signals, e.g., image and audio, and measures the error or distortion between them. In our case, our signal is a frame sequence of images, where we compare a clean sample \mathbf{x} with a distorted (backdoored) sample $\hat{\mathbf{x}}$. In MSE, the error signal is given by $e = \mathbf{x} - \hat{\mathbf{x}}$, which is indeed the difference between pixels for two samples. However, MSE has no context neighbor pixels, which could lead to misleading results [17, 49]. For instance, a blurry image with an MSE score of 0.2, i.e., 20% of the pixels are modified, and a square of 20% of the sample size on top of the image would give the same MSE value. However, the blurry image is recognizable while the other is not. That is, two differently distorted images could have the same MSE for some perturbations more visible than others. Therefore, MSE cannot be the best measurement for backdoor attacks. Still, it could provide sufficient insights for quantifying stealthiness.

To overcome the locality of MSE, Wang et al. [50] proposed a measure for structural similarity index (SSIM) that compares local patterns of pixel intensities rather than single pixels, as in MSE. Images are highly structured, whereas pixels exhibit strong dependencies carrying meaningful information. SSIM computes the changes between two windows instead of the pixel-by-pixel calculations given by

$$SSIM(\mathbf{x}, \hat{\mathbf{x}}) = \frac{(2\mu_{\mathbf{x}}\mu_{\hat{\mathbf{x}}} + c_1)(2\sigma_{\mathbf{x}\hat{\mathbf{x}}} + c_2)}{(\mu_{\mathbf{x}}^2 + \mu_{\hat{\mathbf{x}}}^2 + c_1)(\sigma_{\mathbf{x}}^2 + \sigma_{\hat{\mathbf{x}}}^2 + c_2)},$$

where $\mu_{\mathbf{x}}$ is the pixel sample mean of \mathbf{x} , $\mu_{\hat{\mathbf{x}}}$ is the pixel sample mean of $\hat{\mathbf{x}}$, c_1 and c_2 are two variables to stabilize the division.

5.2 Evaluating Stealthiness

In this section, having analyzed metrics for comparing the variation between the clean and the backdoor images, we select SSIM as the most useful for our case. We evaluate the stealthiness of our different attacks based on the SSIM between the clean and backdoored images. The SSIM values are averaged over 16 (as the batch size) randomly selected images from the test set. Precisely, we compare each clean frame with its each backdoor frame counterpart. Then, the SSIM per frame is averaged. To the best of our knowledge, this is the first application of SSIM for comparing similarities in neuro-morphic data, used for backdoor attacks in SNNs, or used in the SNN domain overall. This addresses Challenge C.4.

5.2.1 Static and Moving Triggers

We first analyze the static and moving triggers in two positions: corner (top-left) and middle, see Figure 7a. We observe that the simpler the dataset, the more the stealthiness reduction, i.e., SSIM is lower. Additionally, the trigger size and the polarity affect the stealthiness. Indeed, the larger the trigger size, the less SSIM, which is expected. However, polarity also plays a crucial role in stealthiness. We observe a noticeable similarity downgrade related to the trigger polarity. The largest similarity degradation is observed for the N-MNIST dataset, with a trigger size of 0.01, and placing the trigger in the top-left corner. The background polarity, i.e., $p = 0$, shows high SSIM; however, with $p = 3$, the SSIM lowers to 94.5. This could be directly linked to the number of pixels of a given polarity in an area. The less polarity in an area, the more “contrast” it would create, being less stealthy.

Lastly, comparing the static and moving triggers, we observe a more significant degradation when the trigger is moving, although it is negligible in some datasets or settings. Triggers in noisy datasets as CIFAR10-DVS, are more tolerable to input perturbations. However, modifications in cleaner datasets, such as N-MNIST, significantly change the image’s overall structure, achieving a lower SSIM.

5.2.2 Smart Triggers

Smart triggers select the trigger polarity and location by themselves, based on the image’s least or most active area and the least prominent polarity in an area. We observe a larger degradation based on the trigger size and when placed in the least active area (see Figure 7b). This is expected as the trigger in the most active area gets hidden by the high activity, i.e., motion. Thus, the performance of triggers in the most active area gets lowered but gains trigger stealthiness, which must be considered a trade-off between stealthiness and performance.

5.2.3 Dynamic Triggers

Lastly, dynamic triggers (see Figure 7c) show impressive stealthiness as γ gets smaller, even to the point of being indistinguishable from the clean image. We also observe that the more complex the dataset, the less the reduction in the stealthiness, contrary to N-MNIST, where the degradation is notable with $\gamma = 0.1$. This effect is related to the number of pixel changes and the noise in the data. A dataset with large noise has much activity, thus being easier for the trigger to be hidden, as in CIFAR10-DVS. However, with “clean” datasets that contain little noise as N-MNIST, even the subtlest perturbation makes a noticeable change. Still, with $\gamma = 0.01$, the perturbation in every tested dataset is invisible.

6 Related Work

6.1 SNNs

SNNs are artificial neural networks inspired by how the neurons in the brain work. In recent years, numerous efforts have been made to develop supervised learning algorithms for SNNs to make them more practical and widely applicable. One of the first such algorithms was Spike Prop [4], which was based on backpropagation and could be used to train single-layer SNNs. However, it was not until more recent developments that SNNs could be applied to multi-layer setups. Despite such advances, most existing SNN training methods still require manual tuning of the spiking neuron membrane, which can be time-consuming and may limit the performance of the SNN. To overcome this limitation, Fang et al. [13] proposed a method that can learn the weights and hyperparameters of the membranes in an automated way, thus eliminating the need for manual tuning. This advancement

may make SNNs more practical and easier to use for a broader range of applications.

Several other notable developments in the field of SNNs are worth mentioning. One such development is event-driven update rules, allowing SNNs to operate more efficiently by only updating the network when necessary [54]. This contrasts traditional neural networks that require continuous updates and can be computationally expensive. Another area of research in SNNs is structural plasticity, which refers to the network’s ability to change its structure during training [51, 54]. This can be accomplished through the addition or removal of connections between neurons or through the creation of new neurons altogether. Structural plasticity can improve the learning efficiency and generalization capabilities of SNNs and is effective in various tasks. There are also ongoing efforts to develop unsupervised learning algorithms for SNNs, allowing them to learn from data without needing labeled examples [23]. Unsupervised learning is a critical component of the brain’s learning process and can significantly expand the range of tasks that SNNs can perform.

6.2 Backdoor Attacks

Backdoor attacks were first introduced by Gu et al., where the authors presented BadNets [20]. BadNets uses a square-shaped trigger on a fixed location to inject the backdoor task; it was the first to show backdoor vulnerabilities in machine learning. BadNets requires access to the training data for injecting the backdoor, contrary to the work by Liu et al. [34], which alleviated this assumption. The authors presented a novel work where access to the training data was not needed. The authors systematically reconstructed training samples to inject the backdoor by adding the trigger on top of the samples and retraining the model.

The abovementioned approaches use static triggers, i.e., the trigger is in the exact location for all the samples. Nguyen and Tran [37] developed a dynamic backdoor attack in which the trigger varies with the input. Specifically, a generator creates a pixel scatter that is then overlapped with the clean input. A similar approach was investigated by Salem et al. [39], who also constructed a dynamic backdoor attack. However, instead of a pixel-scattered trigger, the trigger is a square, which has the advantage of applying it to physical objects.

Aiming to increase the stealthiness of the backdoor, Lie et al. created ReFool [35], which includes benign-looking triggers, as reflections, in the clean sample. A similar approach was followed by Zhang et al. [55], who proposed Poison Ink, where the image structure of the image is extracted. The structure is then injected with a crafted pixel pattern and included in the clean image. The resulting poisoned image is indistinguishable from the clean sample.

In the area of SNNs and neuromorphic datasets, only [1] explored backdoor attacks. However, their experimentation is limited to exploring static and moving triggers using simple

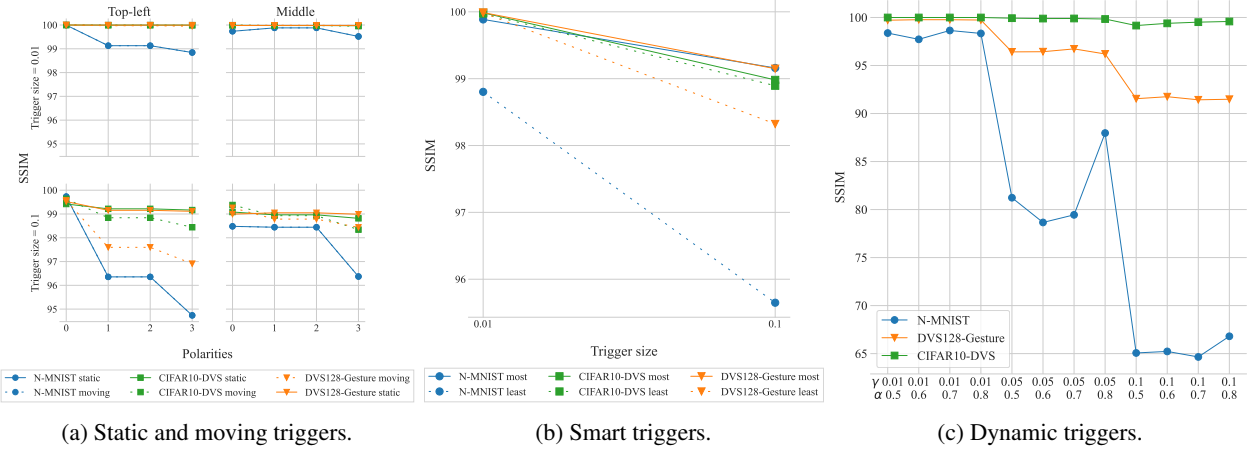


Figure 7: SSIM of different triggers.

datasets and models. Moreover, they do not detail the core reasoning behind backdoors in SNN. We extend the previous work by obtaining better ASR in the same settings, exploring novel backdoor injection methods, and assessing their performance in the presence of defenses.

6.3 Defenses Against Backdoor Attacks

Backdoor attacks can be mitigated using either model-based or data-based defenses. Model-based defenses involve examining potentially infected models to identify and reconstruct the backdoor trigger. An example is Neural Cleanse (NC) [47], which aims to reconstruct the smallest trigger capable of causing the model to misclassify a specific input. This approach is based on the premise that an infected model is more likely to misclassify an input with a trigger than one that does not have a trigger. Another model-based approach is ABS [33], which involves activating every model neuron and analyzing anomalies in the resulting output. Model-based defenses are designed to specifically target infected models, searching for signs of a trigger and attempting to reconstruct it. This approach is effective because the presence of a trigger is often a reliable indicator that the model has been compromised. However, it is also possible for a model to be infected without a trigger, where they are not applicable. Thus, model-based countermeasures are limited to cases with triggers.

Data-based defenses aim to detect the presence of a backdoor by analyzing the dataset without inspecting the model itself. One approach in this category is clustering techniques to differentiate between clean and poisoned data [7]. Another approach, STRIP [14], combines the provided dataset with known infected data and queries the model on the resulting combined dataset. By measuring the entropy of the model’s output on this combined dataset, STRIP can detect backdoored inputs, which tend to have lower entropy than clean inputs. Data-based defenses focus on analyzing the

dataset to detect the presence of a backdoor. These approaches are helpful because they do not require knowledge of the specific trigger used to infect the model, making them more robust against variations in the method of infection. However, data-based defenses may not be as effective at detecting more subtle forms of backdoor attacks, which may not leave as clear a signature in the dataset.

Currently, no defenses are SNN or neuromorphic data-specific. As we have shown, some well-performing defenses adapted from the image domain do not work well in SNNs. Developing SNNs or neuromorphic data-specific countermeasures is necessary for future research.

7 Conclusions & Future Work

The wide usage of DNNs in multiple tasks has led to their security evaluations. However, emerging technologies, such as SNNs, are gaining importance but have not been much evaluated against security threats. In this paper, we investigate backdoor attacks in SNNs using neuromorphic data. We propose different attack methods, even an invisible dynamic trigger that changes with time and is undetectable under human inspection. Furthermore, we evaluate these new attacks against (adapted by us) state-of-the-art defenses from the image domain. We show that our attacks could achieve up to 100% ASR without noticeable clean accuracy degradation, even when the defenses are applied.

Our investigation shows that SNNs are vulnerable to backdoor attacks and that current defenses must be improved. Developing SNNs and neuromorphic data-specific countermeasures is an important future line of research. SNNs are also emerging in other domains like the graph domain, where backdoor attacks are becoming more important. Backdoor attacks in spiking graph neural networks have challenges, which could require specific backdoor designs. Lastly, other common threats to DNNs could also be adapted to SNNs, e.g.,

inference attacks and adversarial examples. For example, data reconstruction from a trained model has been well-explored but is yet unknown if neuromorphic data could be recovered.

References

- [1] Gorka Abad, Oguzhan Ersoy, Stjepan Picek, Víctor Julio Ramírez-Durán, and Aitor Urbieta. Poster: Backdoor attacks on spiking nns and neuromorphic datasets. In *Proceedings of the 2022 ACM SIGSAC Conference on Computer and Communications Security*, pages 3315–3317, 2022.
- [2] Philipp Akopyan, Jun Sawada, Andrew Cassidy, Rodrigo Alvarez-Icaza, John Arthur, Paul Merolla, Nabil Imam, Yutaka Nakamura, Pallab Datta, Gi-Joon Nam, Brian Taba, Michael Beakes, Bernard Brezzo, Jente B. Kuang, Rajit Manohar, William P. Risk, Bryan Jackson, and Dharmendra S. Modha. Truenorth: Design and tool flow of a 65 mw 1 million neuron programmable neurosynaptic chip. *IEEE Transactions on Computer-Aided Design of Integrated Circuits and Systems*, 34(10):1537–1557, 2015.
- [3] Arnon Amir, Brian Taba, David Berg, Timothy Melano, Jeffrey McKinstry, Carmelo Di Nolfo, Tapan Nayak, Alexander Andreopoulos, Guillaume Garreau, Marcela Mendoza, et al. A low power, fully event-based gesture recognition system. In *Proceedings of the IEEE conference on computer vision and pattern recognition*, pages 7243–7252, 2017.
- [4] Sander M Bohte, Joost N Kok, and Han La Poutre. Error-backpropagation in temporally encoded networks of spiking neurons. *Neurocomputing*, 48(1-4):17–37, 2002.
- [5] Tom Brown, Benjamin Mann, Nick Ryder, Melanie Subbiah, Jared D Kaplan, Prafulla Dhariwal, Arvind Neelakantan, Pranav Shyam, Girish Sastry, Amanda Askell, et al. Language models are few-shot learners. *Advances in neural information processing systems*, 33:1877–1901, 2020.
- [6] Nicholas Carlini, Florian Tramer, Eric Wallace, Matthew Jagielski, Ariel Herbert-Voss, Katherine Lee, Adam Roberts, Tom Brown, Dawn Song, Ulfar Erlingsson, et al. Extracting training data from large language models. In *30th USENIX Security Symposium (USENIX Security 21)*, pages 2633–2650, 2021.
- [7] Bryant Chen, Wilka Carvalho, Nathalie Baracaldo, Heiko Ludwig, Benjamin Edwards, Taesung Lee, Ian Molloy, and Biplav Srivastava. Detecting backdoor attacks on deep neural networks by activation clustering. *arXiv preprint arXiv:1811.03728*, 2018.
- [8] Guang Chen, Hu Cao, Jorg Conradt, Huajin Tang, Florian Rohrbein, and Alois Knoll. Event-based neuromorphic vision for autonomous driving: A paradigm shift for bio-inspired visual sensing and perception. *IEEE Signal Processing Magazine*, 37(4):34–49, 2020.
- [9] Payal Dhar. The carbon impact of artificial intelligence. *Nat. Mach. Intell.*, 2(8):423–425, 2020.
- [10] Khoa Doan, Yingjie Lao, Weijie Zhao, and Ping Li. Lira: Learnable, imperceptible and robust backdoor attacks. In *Proceedings of the IEEE/CVF International Conference on Computer Vision*, pages 11966–11976, 2021.
- [11] Jason K Eshraghian, Max Ward, Emre Neftci, Xinxin Wang, Gregor Lenz, Girish Dwivedi, Mohammed Benamoun, Doo Seok Jeong, and Wei D Lu. Training spiking neural networks using lessons from deep learning. *arXiv preprint arXiv:2109.12894*, 2021.
- [12] Wei Fang, Yanqi Chen, Jianhao Ding, Ding Chen, Zhaofei Yu, Huihui Zhou, Yonghong Tian, and other contributors. Spikingjelly. <https://github.com/fangwei123456/spikingjelly>, 2020. Accessed: 2022-10-12.
- [13] Wei Fang, Zhaofei Yu, Yanqi Chen, Timothée Masquelier, Tiejun Huang, and Yonghong Tian. Incorporating learnable membrane time constant to enhance learning of spiking neural networks. In *Proceedings of the IEEE/CVF International Conference on Computer Vision*, pages 2661–2671, 2021.
- [14] Yansong Gao, Change Xu, Derui Wang, Shiping Chen, Damith C Ranasinghe, and Surya Nepal. Strip: A defense against trojan attacks on deep neural networks. In *Proceedings of the 35th Annual Computer Security Applications Conference*, pages 113–125, 2019.
- [15] Samanwoy Ghosh-Dastidar and Hojjat Adeli. Improved spiking neural networks for eeg classification and epilepsy and seizure detection. *Integr. Comput.-Aided Eng.*, 14(3):187–212, aug 2007.
- [16] Samanwoy Ghosh-Dastidar and Hojjat Adeli. Spiking neural networks. *International journal of neural systems*, 19(04):295–308, 2009.
- [17] Bernd Girod. What’s wrong with mean-squared error? *Digital images and human vision*, pages 207–220, 1993.
- [18] Ian Goodfellow, Yoshua Bengio, and Aaron Courville. *Deep Learning*. MIT Press, 2016. <http://www.deeplearningbook.org>.
- [19] Alex Graves, Abdel-rahman Mohamed, and Geoffrey Hinton. Speech recognition with deep recurrent neural networks. In *2013 IEEE international conference on*

acoustics, speech and signal processing, pages 6645–6649. Ieee, 2013.

[20] Tianyu Gu, Kang Liu, Brendan Dolan-Gavitt, and Siddharth Garg. Badnets: Evaluating backdooring attacks on deep neural networks. *IEEE Access*, 7:47230–47244, 2019.

[21] Ankur Gupta and Lyle N. Long. Character recognition using spiking neural networks. In *2007 International Joint Conference on Neural Networks*, pages 53–58, 2007.

[22] S Han, H Mao, and WJ Dally. Compressing deep neural networks with pruning, trained quantization and huffman coding. arxiv 2015. *arXiv preprint arXiv:1510.00149*.

[23] Hananel Hazan, Daniel Saunders, Darpan T Sanghavi, Hava Siegelmann, and Robert Kozma. Unsupervised learning with self-organizing spiking neural networks. In *2018 International Joint Conference on Neural Networks (IJCNN)*, pages 1–6. IEEE, 2018.

[24] Matthew Jagielski, Nicholas Carlini, David Berthelot, Alex Kurakin, and Nicolas Papernot. High accuracy and high fidelity extraction of neural networks. In *29th USENIX security symposium (USENIX Security 20)*, pages 1345–1362, 2020.

[25] Alex Krizhevsky, Geoffrey Hinton, et al. Learning multiple layers of features from tiny images. 2009.

[26] Alex Krizhevsky, Ilya Sutskever, and Geoffrey E Hinton. Imagenet classification with deep convolutional neural networks. *Advances in neural information processing systems*, 25, 2012.

[27] Souvik Kundu, Gourav Datta, Massoud Pedram, and Peter A Beerel. Spike-thrift: Towards energy-efficient deep spiking neural networks by limiting spiking activity via attention-guided compression. In *Proceedings of the IEEE/CVF WACV*, pages 3953–3962, 2021.

[28] Yann LeCun. The mnist database of handwritten digits. <http://yann.lecun.com/exdb/mnist/>, 1998.

[29] Jun Haeng Lee, Tobi Delbrück, and Michael Pfeiffer. Training deep spiking neural networks using backpropagation. *Frontiers in neuroscience*, 10:508, 2016.

[30] Hongmin Li, Hanchao Liu, Xiangyang Ji, Guoqi Li, and Luping Shi. Cifar10-dvs: an event-stream dataset for object classification. *Frontiers in neuroscience*, 11:309, 2017.

[31] Kang Liu, Brendan Dolan-Gavitt, and Siddharth Garg. Fine-pruning: Defending against backdooring attacks on deep neural networks. In *International Symposium on Research in Attacks, Intrusions, and Defenses*, pages 273–294. Springer, 2018.

[32] Shih-Chii Liu, Bodo Rueckauer, Enea Ceolini, Adrian Huber, and Tobi Delbrück. Event-driven sensing for efficient perception: Vision and audition algorithms. *IEEE Signal Processing Magazine*, 36(6):29–37, 2019.

[33] Yingqi Liu, Wen-Chuan Lee, Guanhong Tao, Shiqing Ma, Yousra Aafer, and Xiangyu Zhang. Abs: Scanning neural networks for back-doors by artificial brain stimulation. In *Proceedings of the 2019 ACM SIGSAC Conference on Computer and Communications Security*, pages 1265–1282, 2019.

[34] Yingqi Liu, Shiqing Ma, Yousra Aafer, Wen-Chuan Lee, Juan Zhai, Weihang Wang, and Xiangyu Zhang. Trojaning attack on neural networks. 2017.

[35] Yunfei Liu, Xingjun Ma, James Bailey, and Feng Lu. Reflection backdoor: A natural backdoor attack on deep neural networks. In *European Conference on Computer Vision*, pages 182–199. Springer, 2020.

[36] Ana I Maqueda, Antonio Loquercio, Guillermo Gallego, Narciso García, and Davide Scaramuzza. Event-based vision meets deep learning on steering prediction for self-driving cars. In *Proceedings of the IEEE conference on computer vision and pattern recognition*, pages 5419–5427, 2018.

[37] Tuan Anh Nguyen and Anh Tran. Input-aware dynamic backdoor attack. *Advances in Neural Information Processing Systems*, 33:3454–3464, 2020.

[38] Garrick Orchard, Ajinkya Jayawant, Gregory K Cohen, and Nitish Thakor. Converting static image datasets to spiking neuromorphic datasets using saccades. *Frontiers in neuroscience*, 9:437, 2015.

[39] Ahmed Salem, Rui Wen, Michael Backes, Shiqing Ma, and Yang Zhang. Dynamic backdoor attacks against machine learning models. In *2022 IEEE 7th European Symposium on Security and Privacy (EuroS&P)*, pages 703–718. IEEE, 2022.

[40] Ali Samadzadeh, Fatemeh Sadat Tabatabaei Far, Ali Javadi, Ahmad Nickabadi, and Morteza Haghir Chehreghani. Convolutional spiking neural networks for spatio-temporal feature extraction. *arXiv preprint arXiv:2003.12346*, 2020.

[41] Teresa Serrano-Gotarredona and Bernabé Linares-Barranco. A 128×128 1.5% contrast sensitivity 0.9% fpn 3 μ s latency 4 mw asynchronous frame-free dynamic vision sensor using transimpedance preamplifiers. *IEEE Journal of Solid-State Circuits*, 48(3):827–838, 2013.

[42] Christian Szegedy, Wojciech Zaremba, Ilya Sutskever, Joan Bruna, Dumitru Erhan, Ian Goodfellow, and Rob Fergus. Intriguing properties of neural networks. *arXiv preprint arXiv:1312.6199*, 2013.

[43] Amirhossein Tavanaei, Masoud Ghodrati, Saeed Reza Kheradpisheh, Timothée Masquelier, and Anthony Maida. Deep learning in spiking neural networks. *Neural networks*, 111:47–63, 2019.

[44] Amirhossein Tavanaei, Masoud Ghodrati, Saeed Reza Kheradpisheh, Timothée Masquelier, and Anthony Maida. Deep learning in spiking neural networks. *Neural Networks*, 111:47–63, mar 2019.

[45] Alexander Turner, Dimitris Tsipras, and Aleksander Madry. Clean-label backdoor attacks. 2018.

[46] Alberto Viale, Alberto Marchisio, Maurizio Martina, Guido Masera, and Muhammad Shafique. Carsnn: An efficient spiking neural network for event-based autonomous cars on the loihi neuromorphic research processor. In *2021 International Joint Conference on Neural Networks (IJCNN)*, pages 1–10. IEEE, 2021.

[47] Bolun Wang, Yuanshun Yao, Shawn Shan, Huiying Li, Bimal Viswanath, Haitao Zheng, and Ben Y Zhao. Neural cleanse: Identifying and mitigating backdoor attacks in neural networks. In *2019 IEEE Symposium on Security and Privacy (SP)*, pages 707–723. IEEE, 2019.

[48] Zhou Wang and Alan C Bovik. Mean squared error: Love it or leave it? a new look at signal fidelity measures. *IEEE signal processing magazine*, 26(1):98–117, 2009.

[49] Zhou Wang, Alan C Bovik, and Ligang Lu. Why is image quality assessment so difficult? In *2002 IEEE International conference on acoustics, speech, and signal processing*, volume 4, pages IV–3313. IEEE, 2002.

[50] Zhou Wang, Alan C Bovik, Hamid R Sheikh, and Eero P Simoncelli. Image quality assessment: from error visibility to structural similarity. *IEEE transactions on image processing*, 13(4):600–612, 2004.

[51] Mahima Milinda Alwis Weerasinghe, Josafath I Espinosa-Ramos, Grace Y Wang, and Dave Parry. Incorporating structural plasticity approaches in spiking neural networks for eeg modelling. *IEEE Access*, 9:117338–117348, 2021.

[52] Simei Gomes Wysoski, Lubica Benuskova, and Nikola Kasabov. Evolving spiking neural networks for audiovisual information processing. *Neural Networks*, 23(7):819–835, 2010.

[53] Jiecao Yu, Andrew Lukefahr, David Palframan, Ganesh Dasika, Reetuparna Das, and Scott Mahlke. Scalpel: Customizing dnn pruning to the underlying hardware parallelism. *ACM SIGARCH Computer Architecture News*, 45(2):548–560, 2017.

[54] Anguo Zhang, Xumin Li, Yueming Gao, and Yuzhen Niu. Event-driven intrinsic plasticity for spiking convolutional neural networks. *IEEE Transactions on Neural Networks and Learning Systems*, 33(5):1986–1995, 2021.

[55] Jie Zhang, Chen Dongdong, Qidong Huang, Jing Liao, Weiming Zhang, Huamin Feng, Gang Hua, and Nenghai Yu. Poison ink: Robust and invisible backdoor attack. *IEEE Transactions on Image Processing*, 31:5691–5705, 2022.

[56] Alex Zihao Zhu, Dinesh Thakur, Tolga Özslan, Bernd Pfommer, Vijay Kumar, and Kostas Daniilidis. The multivehicle stereo event camera dataset: An event camera dataset for 3d perception. *IEEE Robotics and Automation Letters*, 3(3):2032–2039, 2018.

A Additional Experiments

A.1 Results for Static and Moving Backdoors

In Figures 8 and 9, we provide results for static backdoors and moving backdoors, respectively.

A.2 Clean Accuracy Degradation of Static Triggers

The clean accuracy degradation after the static attack in the bottom-right corner is shown in Figure 10, for the middle trigger see Figure 11. Lastly, the degradation in the top-left corner is shown in Figure 12.

A.3 Clean Accuracy Degradation of Moving Triggers

The clean accuracy degradation after the moving attack in the bottom-right corner is shown in Figure 13, for the middle trigger see Figure 14. Lastly, the degradation in the top-left corner is shown in Figure 15.

A.4 Clean Accuracy Degradation of Smart Triggers

The clean accuracy degradation of the smart attack in the most active area and the least active trigger is shown in Figure 16. For the least active area and the least active trigger, see Figure 17. For the most active triggers in the most and least active areas, see Figure 18 and Figure 19, respectively.

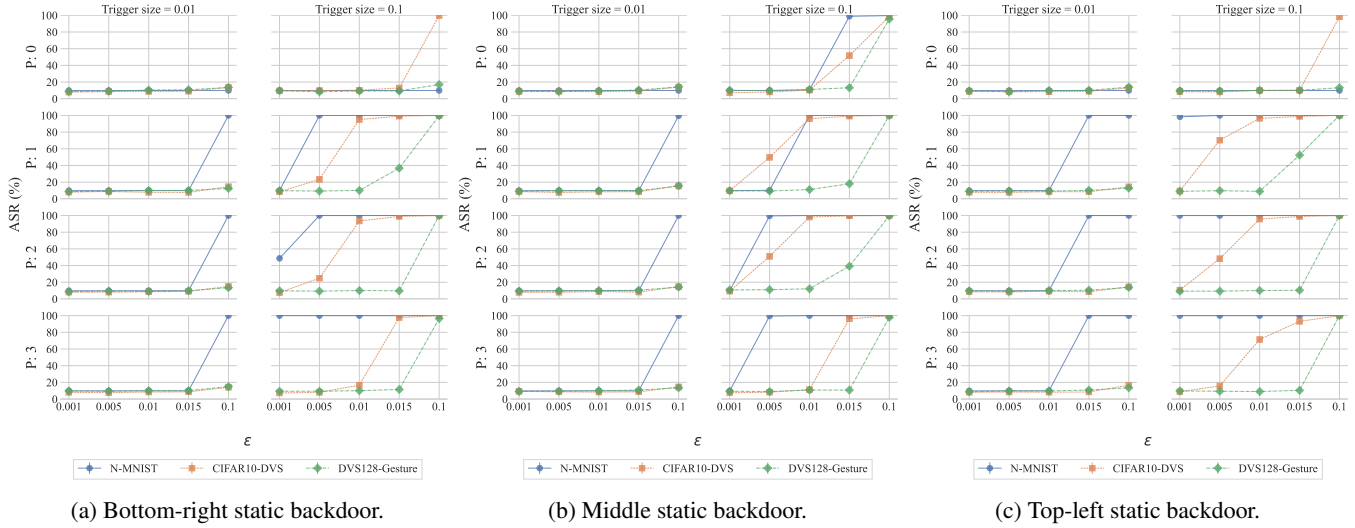


Figure 8: ASR of static triggers.

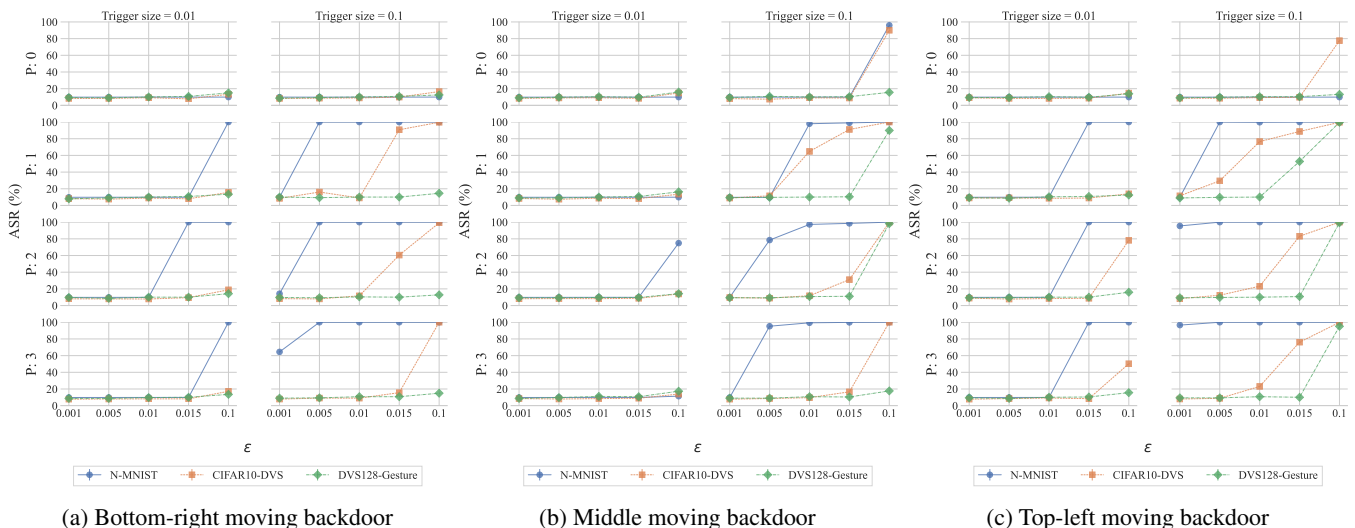


Figure 9: ASR of moving triggers.

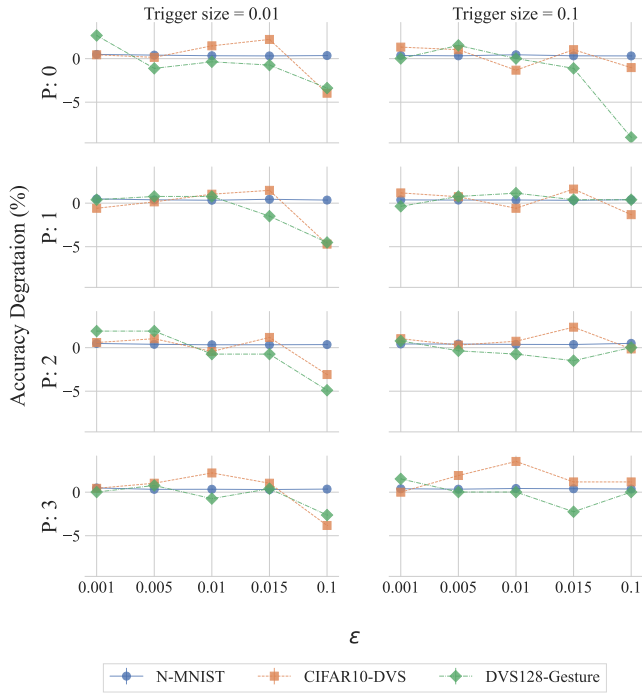


Figure 10: Bottom-right static trigger clean accuracy degradation.

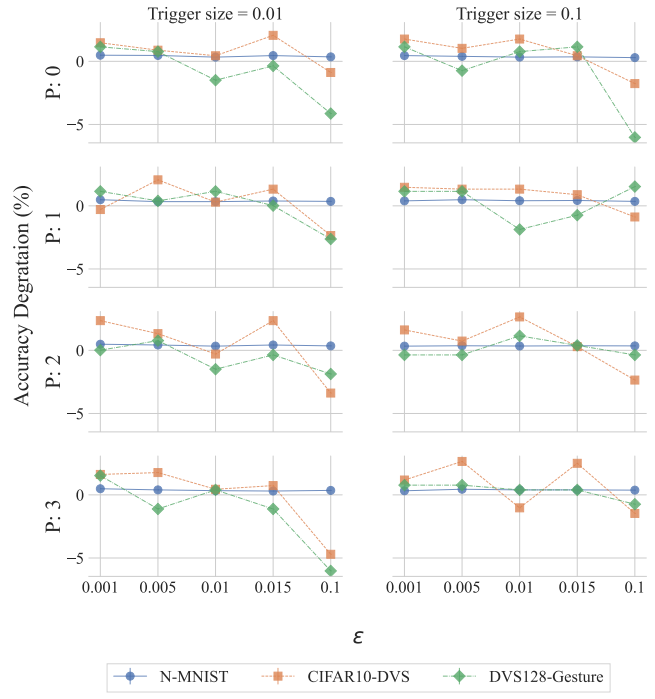


Figure 12: Top-left static trigger clean accuracy degradation.

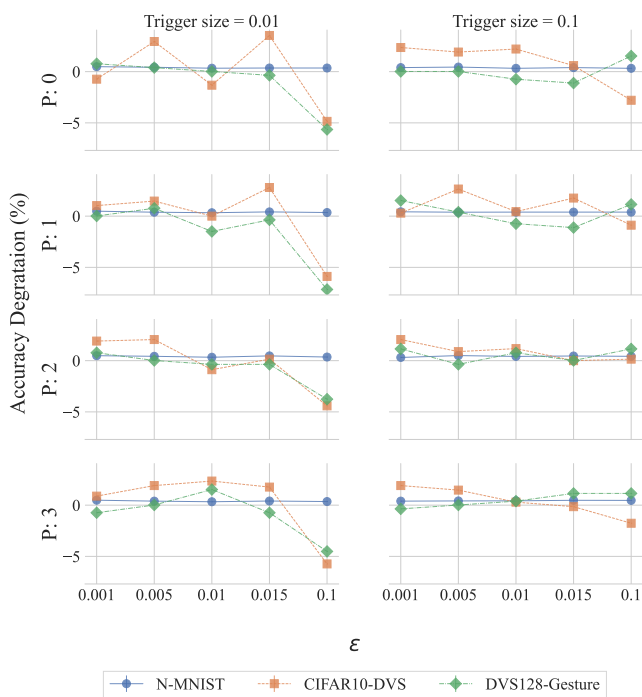


Figure 11: Middle static trigger clean accuracy degradation.

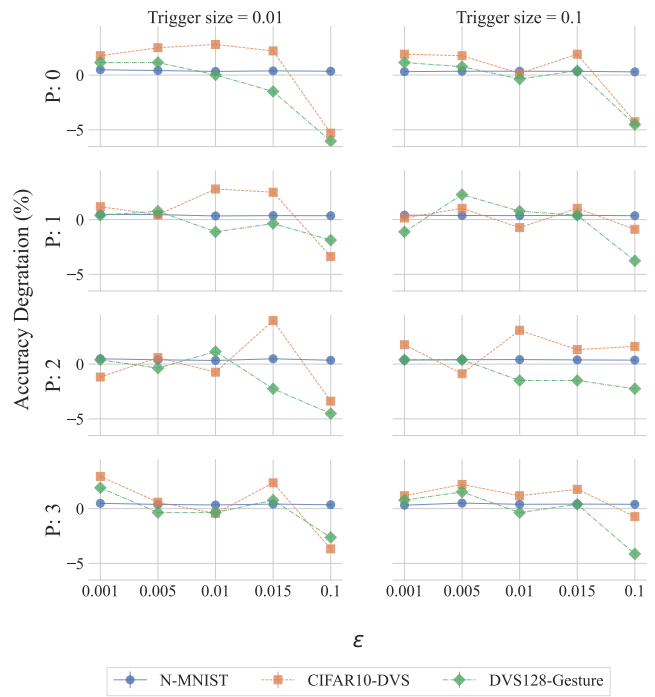


Figure 13: Bottom-right moving trigger clean accuracy degradation.

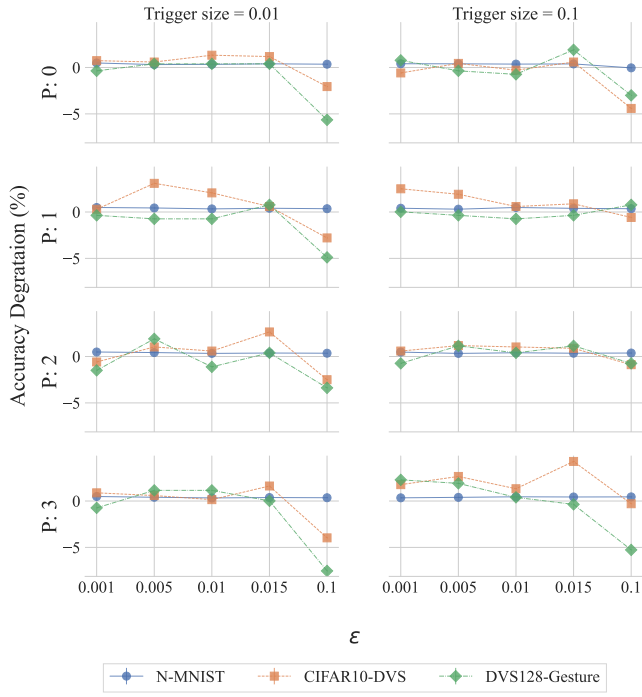


Figure 14: Middle moving trigger clean accuracy degradation.

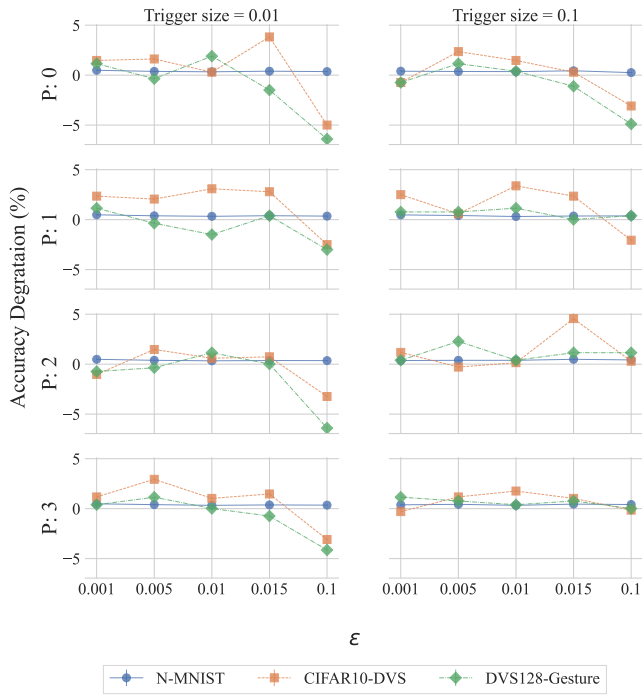


Figure 15: Top-left moving trigger clean accuracy degradation.

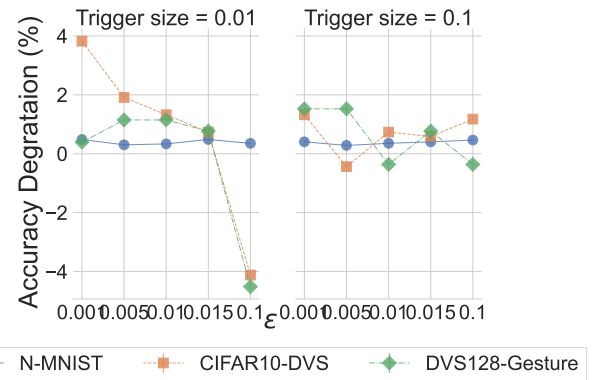


Figure 16: Clean accuracy degradation of the smart trigger in the most active area and least active trigger.

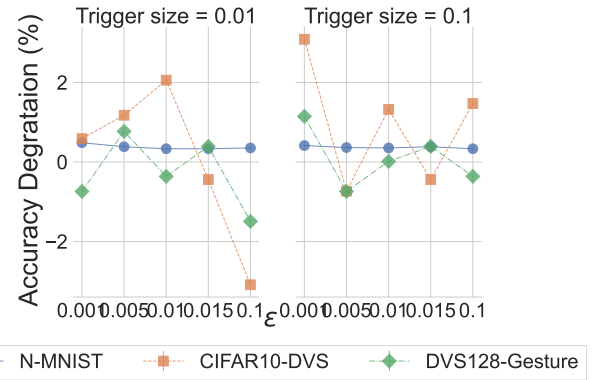


Figure 17: Clean accuracy degradation of the smart trigger in the least active area and least active trigger.

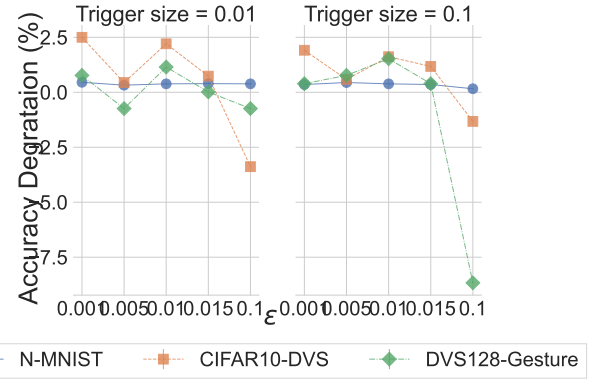


Figure 18: Clean accuracy degradation of the smart trigger in the most active area and most active trigger.

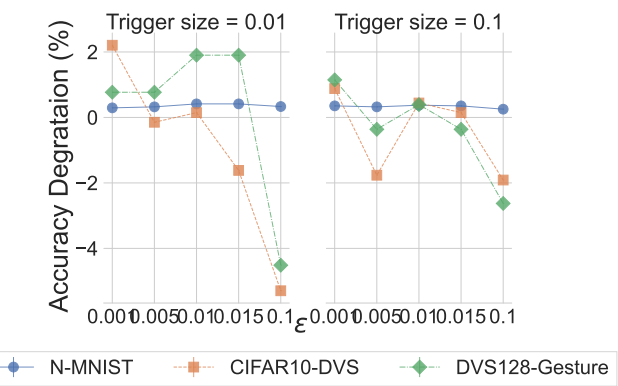


Figure 19: Clean accuracy degradation of the smart trigger in the least active area and most active trigger.